

Creation of particle-hole superposition states in graphene at multiphoton resonant excitation by laser radiation

H. K. Avetissian,^{*} A. K. Avetissian, G. F. Mkrtchian, and Kh. V. Sedrakian

Centre of Strong Fields Physics, Yerevan State University, 1 A. Manukian, Yerevan 0025, Armenia

(Received 24 November 2011; revised manuscript received 10 February 2012; published 29 March 2012)

Nonlinear dynamics of the establishment of electron-hole coherent superposition states in graphene by multiphoton resonant excitation of interband transitions in laser fields is considered. The single-particle time-dependent density matrix for such a quantized system is calculated in the multiphoton resonant approximation. The dependence of Rabi oscillations of the Fermi-Dirac sea in graphene on the time, momentum, and photon number at multiphoton laser excitation is analyzed.

DOI: [10.1103/PhysRevB.85.115443](https://doi.org/10.1103/PhysRevB.85.115443)

PACS number(s): 78.67.Wj, 42.50.Hz, 78.47.jh, 03.65.Pm

I. INTRODUCTION

Graphene, a single sheet of carbon atoms in a honeycomb lattice, has attracted an enormous amount of interest since its experimental discovery and isolation.^{1,2} Its quasiparticle states behave like massless “relativistic” Dirac fermions^{3,4} and obey a two-dimensional Dirac equation, where the light speed is replaced by the Fermi velocity, which is 300 times smaller than the light speed in vacuum. In addition to various applications in electronic devices, graphene physics opens up a wide research field unifying low-energy condensed-matter physics and quantum electrodynamics (QED).^{5–9} Many fundamental nonlinear QED processes, specifically electron-positron pair production in superstrong laser fields of ultrarelativistic intensities,¹⁰ the observation of which remains problematic even in the current superintense laser fields, have their counterparts in graphene where considerably weaker electromagnetic fields are required for experimental realization of “antimatter” production from vacuum. In this connection, one can note the Klein paradox,^{11–13} the Schwinger mechanism,^{14–16} and zitterbewegung^{17–20} for particle-hole excitation, as well as diverse physical and applied effects based on zitterbewegung, e.g., minimal conductivity at vanishing carrier concentration,^{21,22} etc.

Due to a massless energy spectrum, the Compton wavelength for a graphene quasiparticle tends to infinity. On the other hand, in QED the Compton wavelength is the characteristic length below which the single-particle concept is no longer valid, and spontaneous particle-antiparticle pair creation or annihilation occurs permanently. Therefore, at the interaction of an electromagnetic field with intrinsic graphene, there is no quasiclassical limit because no matter how weak the applied field is and how small the photon energy is, the particle-hole pairs will be created during the whole interaction process—at arbitrary distances.

In graphene, wave-particle interaction can be characterized by the dimensionless parameter

$$\chi = \frac{eE v_F}{\omega \hbar \omega},$$

which represents the work of the wave electric field E on a period $1/\omega$ in units of photon energy $\varepsilon_\gamma = \hbar\omega$. Here v_F is the Fermi velocity ($v_F \approx c/300$) and e is the elementary charge. The average intensity of the wave expressed by χ can

be estimated as

$$I_\chi = \chi^2 \times 3.07 \times 10^{11} \text{ W cm}^{-2} (\hbar\omega/\text{eV})^4.$$

Depending on the value of this parameter χ , one can distinguish three different regimes in the wave-particle interaction process. Thus, $\chi \ll 1$ corresponds to the one-photon interaction regime, $\chi \sim 1$ to the multiphoton interaction regime, and $\chi \gg 1$ corresponds to the static field limit or the Schwinger regime. As is seen, the intensity I_χ depends strongly on the photon energy. In particular, for infrared photons, $\varepsilon_\gamma \sim 0.1$ eV, the multiphoton interaction regime can be achieved at the intensities $I_\chi = 3.07 \times 10^7 \text{ W cm}^{-2}$. Note that in the case of free electrons at the same photon energies, multiphoton effects take place at the intensities $I \sim 10^{16} \text{ W cm}^{-2}$.¹⁰ Such a huge difference, as well as the gapless particle-hole energy spectrum in graphene, make another interesting nonlinear QED process realistic, namely the multiphoton excitation of Dirac vacuum with Rabi oscillations at ultrafast time scales.²³

In the present work, the microscopic theory of the creation of particle-hole coupled states in graphene via multiphoton resonant excitation by laser fields is developed. It is well known that Rabi oscillation of states’ populations is the coherent response of two-level atomic systems under resonant excitation. The one-photon resonant excitation of atoms and associated Rabi oscillations have been studied comprehensively both theoretically and experimentally and described in numerous review articles and books (see, e.g., Ref. 24). Similar phenomena have also been observed in semiconductors.²⁵ Recently, the Rabi oscillations in graphene at one-photon interband excitation (at $\chi \ll 1$) and their influence on the dynamic conductivity were investigated in Refs. 26–28. On the other hand, at a wave-particle interaction in graphene due to free-free intraband transitions, we have a situation analogous to resonant excitation of quantum systems with permanent dipole moments, where direct multiphoton transitions are very effective.^{29–32} Hence, the creation of particle-hole coupled states in graphene via multiphoton resonant excitation is of interest. We consider the multiphoton interaction regime and the nonlinear optical response of graphene at $\chi \sim 1$, considering particle-hole quantum dynamics in the vicinity of the K point. Accordingly, the time evolution of the considered process is found using a nonperturbative resonant approach arising from the quantum kinetic equations. The considered process, apart from its fundamental interest, may also have

practical applications. In particular, particle-hole annihilation from the coherent superposition states will cause intense coherent radiation of harmonics of the applied wave field, which is also briefly discussed in the present work. Note that from this point of view, graphene is considered to be a promising material for harmonics generation due to its strongly enhanced nonlinear electromagnetic properties.^{33–36}

As a result, because of inversion symmetry, at the normal incidence of radiation on the uniform graphene layer only odd harmonics are generated. For the generation of even harmonics, one should break this symmetry, which has been done in Refs. 37 and 38, where the microscopic perturbation theory of second-harmonic generation at the oblique incidence of radiation on the graphene has been developed.

The paper is organized as follows. In Sec. II, the set of equations for a single-particle density matrix is formulated. In Sec. III, we present the analytical solution of the stated equations in the multiphoton resonant approximation. In Sec. IV, the results of numerical integration of basic equations are presented. Finally, conclusions are given in Sec. V.

II. BASIC MODEL AND EVOLUTIONARY EQUATION FOR THE SINGLE-PARTICLE DENSITY MATRIX

Let graphene interact with plane quasimonochromatic laser radiation of carrier frequency ω and slowly varying envelope. To clarify the problem presented in this paper regarding the creation of coherent superposition states, we consider the interaction when the laser wave propagates in a perpendicular direction to the graphene plane (XY) to exclude the effect of magnetic field. This traveling wave for electrons in graphene becomes a homogeneous time-periodic electric field. It is directed along the X axis with the form (constant phase connected with the position of the wave pulse maximum with respect to graphene plane is set zero)

$$\mathbf{E}(t) = \hat{x}E_0 \cos \omega t. \quad (1)$$

The problem that we attempt to solve in the given field approximation is analogous to Rabi oscillations in two-level atomic systems with permanent dipole moments. In this case, the physical picture of resonant-wave-graphene interaction will be more visible in the length gauge. Therefore, for the interaction Hamiltonian we will use a length gauge describing the interaction by the potential energy. Cast in the second quantization formalism, the Hamiltonian is

$$\hat{H} = \int \hat{\Psi}^\dagger \hat{H}_s \hat{\Psi} dx dy, \quad (2)$$

where $\hat{\Psi}$ is the fermionic field operator and \hat{H}_s is the single-particle Hamiltonian in the external homogeneous electric field (1). Omitting here real spin and valley quantum numbers, the single-particle Hamiltonian in the vicinity of the K point can be written as

$$\hat{H}_s = v_F \begin{pmatrix} 0 & \hat{p}_x - i\hat{p}_y \\ \hat{p}_x + i\hat{p}_y & 0 \end{pmatrix} + \begin{pmatrix} exE & 0 \\ 0 & exE \end{pmatrix}, \quad (3)$$

where $v_F \approx c/300$ is the Fermi velocity (c is the light speed in vacuum) and $\hat{\mathbf{p}} = \{\hat{p}_x, \hat{p}_y\}$ is the electron momentum operator. The first term in Eq. (3) is the Hamiltonian of a

two-dimensional massless Dirac fermion, and the second term is the interaction part.

We write the fermionic field operator in the form of an expansion in the free Dirac states:

$$\hat{\Psi}(x, y, t) = \sum_{\mathbf{p}, \sigma} \hat{a}_{\mathbf{p}, \sigma}(t) \Psi_{\mathbf{p}, \sigma}(x, y), \quad (4)$$

where the creation and annihilation operators, $\hat{a}_{\mathbf{p}, \sigma}^+(t)$ and $\hat{a}_{\mathbf{p}, \sigma}(t)$, associated with positive ($\sigma = 1$) and negative ($\sigma = -1$) energy solutions satisfy the anticommutation rules at equal times:

$$\{\hat{a}_{\mathbf{p}, \sigma}^\dagger(t), \hat{a}_{\mathbf{p}', \sigma'}(t')\}_{t=t'} = \delta_{\mathbf{p}, \mathbf{p}'} \delta_{\sigma, \sigma'}, \quad (5)$$

$$\{\hat{a}_{\mathbf{p}, \sigma}^\dagger(t), \hat{a}_{\mathbf{p}', \sigma'}^\dagger(t')\}_{t=t'} = \{\hat{a}_{\mathbf{p}, \sigma}(t), \hat{a}_{\mathbf{p}', \sigma'}(t')\}_{t=t'} = 0. \quad (6)$$

The free Dirac solutions corresponding to energies $\mathcal{E}_\sigma = \sigma v_F \sqrt{p_x^2 + p_y^2}$ ($\sigma = \pm 1$) are

$$\Psi_{\mathbf{p}, \sigma}(x, y) = \frac{1}{\sqrt{2S}} \begin{pmatrix} 1 \\ \sigma e^{i\Theta(\mathbf{p})} \end{pmatrix} e^{\frac{i}{\hbar}(p_x x + p_y y)}, \quad (7)$$

where S is the quantization area (graphene layer surface area) and

$$\Theta(\mathbf{p}) = \arctan \left(\frac{p_y}{p_x} \right) \quad (8)$$

is the angle in momentum space.

Taking into account Eqs. (1)–(8), the second quantized Hamiltonian can be expressed in the form

$$\begin{aligned} \hat{H} = & \sum_{\mathbf{p}, \sigma} \mathcal{E}_\sigma(p) \hat{a}_{\mathbf{p}, \sigma}^+ \hat{a}_{\mathbf{p}, \sigma} \\ & + eE(t) \sum_{\mathbf{p}, \sigma} \sum_{\mathbf{p}', \sigma'} D_{\sigma\sigma'}(\mathbf{p}, \mathbf{p}') \hat{a}_{\mathbf{p}, \sigma}^+ \hat{a}_{\mathbf{p}', \sigma'}, \end{aligned} \quad (9)$$

where

$$\begin{aligned} D_{\sigma\sigma'}(\mathbf{p}, \mathbf{p}') = & \frac{1}{2S} [1 + \sigma\sigma' e^{i[\Theta(\mathbf{p}') - \Theta(\mathbf{p})]}] \\ & \times \int x e^{\frac{i}{\hbar}(p'_x - p_x)x + \frac{i}{\hbar}(p'_y - p_y)y} dx dy. \end{aligned} \quad (10)$$

We will use the Heisenberg representation, where the evolution of the operators is given by the following equation:

$$i\hbar \frac{\partial \hat{L}}{\partial t} = [\hat{L}, \hat{H}], \quad (11)$$

and the expectation values are determined by the initial density matrix \hat{D} :

$$\langle \hat{L} \rangle = \text{Tr}(\hat{D} \hat{L}). \quad (12)$$

The single-particle density matrix in momentum space is defined as

$$\rho_{\sigma_1 \sigma_2}(\mathbf{p}_1, \mathbf{p}_2, t) = \langle \hat{a}_{\mathbf{p}_2, \sigma_2}^+(t) \hat{a}_{\mathbf{p}_1, \sigma_1}(t) \rangle. \quad (13)$$

For the initial state of graphene quasiparticles, we assume an ideal Fermi gas in equilibrium. This means that the initial

single-particle density matrix is diagonal and we have the Fermi-Dirac distribution

$$\rho_{\sigma\sigma'}(\mathbf{p},\mathbf{p}',0) = \frac{1}{1 + e^{\frac{\mathcal{E}_\sigma(\mathbf{p})-\mu}{T}}} \delta_{\mathbf{p},\mathbf{p}'} \delta_{\sigma,\sigma'}. \quad (14)$$

Here μ is the chemical potential and T is the temperature in energy units. Taking into account definition (13), from Eq. (11) one can obtain the evolution equation for the single-particle density matrix:

$$i\hbar \frac{\partial \rho_{\sigma_1\sigma_2}(\mathbf{p}_1,\mathbf{p}_2,t)}{\partial t} = [\mathcal{E}_{\sigma_1}(p_1) - \mathcal{E}_{\sigma_2}(p_2)] \rho_{\sigma_1\sigma_2}(\mathbf{p}_1,\mathbf{p}_2,t) - eE(t) \sum_{\mathbf{p},\sigma} [D_{\sigma\sigma_2}(\mathbf{p},\mathbf{p}_2) \rho_{\sigma_1\sigma}(\mathbf{p}_1,\mathbf{p},t) - D_{\sigma_1\sigma}(\mathbf{p}_1,\mathbf{p}) \rho_{\sigma\sigma_2}(\mathbf{p},\mathbf{p}_2,t)]. \quad (15)$$

Then, taking into account the following relation with the Dirac delta function $\delta(\alpha)$:

$$\int_{-\infty}^{\infty} x e^{-i\alpha x} dx = 2\pi i \frac{\partial}{\partial \alpha} \delta(\alpha)$$

and the substitution

$$\sum_{\mathbf{p}} \rightarrow \frac{S}{(2\pi\hbar)^2} \int d\mathbf{p},$$

we obtain a closed set of equations for the density matrix elements:

$$\frac{\partial \rho_{\sigma,\sigma}(\mathbf{p},\mathbf{p},t)}{\partial t} - eE(t) \frac{\partial \rho_{\sigma,\sigma}(\mathbf{p}_1,\mathbf{p},t)}{\partial p_{1x}} \Big|_{\mathbf{p}_1=\mathbf{p}} - eE(t) \frac{\partial \rho_{\sigma,\sigma}(\mathbf{p},\mathbf{p}_2,t)}{\partial p_{2x}} \Big|_{\mathbf{p}_2=\mathbf{p}} = i \frac{eE(t)}{2} \frac{\partial \Theta(\mathbf{p})}{\partial p_x} [\rho_{\sigma,-\sigma}(\mathbf{p},\mathbf{p},t) - \rho_{-\sigma,\sigma}(\mathbf{p},\mathbf{p},t)], \quad (16)$$

$$\begin{aligned} & \frac{\partial \rho_{\sigma,-\sigma}(\mathbf{p},\mathbf{p},t)}{\partial t} - eE(t) \frac{\partial \rho_{\sigma,-\sigma}(\mathbf{p}_1,\mathbf{p},t)}{\partial p_{1x}} \Big|_{\mathbf{p}_1=\mathbf{p}} - eE(t) \frac{\partial \rho_{\sigma,-\sigma}(\mathbf{p},\mathbf{p}_2,t)}{\partial p_{2x}} \Big|_{\mathbf{p}_2=\mathbf{p}} \\ & = \frac{2}{i\hbar} \mathcal{E}_\sigma(p) \rho_{\sigma,-\sigma}(\mathbf{p},\mathbf{p},t) - \frac{eE(t)}{2i} \frac{\partial \Theta(\mathbf{p})}{\partial p_x} [\rho_{\sigma,\sigma}(\mathbf{p},\mathbf{p},t) - \rho_{-\sigma,-\sigma}(\mathbf{p},\mathbf{p},t)]. \end{aligned} \quad (17)$$

In Eqs. (16) and (17), one can eliminate the terms with partial derivatives $\partial/\partial p_x$ based on their characteristics. The characteristic of these equations is the classical equation of motion:

$$\frac{d\mathbf{p}}{dt} = -e\mathbf{E}(t),$$

with the solution

$$p_x = p_{0x} + p_E(t), \quad p_y = p_{0y}, \quad (18)$$

where

$$p_E(t) = -e \int_0^t E(t') dt' = -\frac{eE_0}{\omega} \sin \omega t$$

is the momentum transferred by the wave field. Thus, with the new variables p_{0x} , p_{0y} , and t , Eqs. (16) and (17) read

$$\frac{\partial \rho_{\sigma,\sigma}(\mathbf{p}_0,\mathbf{p}_0,t)}{\partial t} = \frac{i}{2} F(\mathbf{p}_0,t) [\rho_{\sigma,-\sigma}(\mathbf{p}_0,\mathbf{p}_0,t) - \rho_{-\sigma,\sigma}(\mathbf{p}_0,\mathbf{p}_0,t)], \quad (19)$$

$$\frac{\partial \rho_{\sigma,-\sigma}(\mathbf{p}_0,\mathbf{p}_0,t)}{\partial t} = \frac{2}{i\hbar} \tilde{\mathcal{E}}_\sigma(\mathbf{p}_0,t) \rho_{\sigma,-\sigma}(\mathbf{p}_0,\mathbf{p}_0,t) + \frac{i}{2} F(\mathbf{p}_0,t) [\rho_{\sigma,\sigma}(\mathbf{p}_0,\mathbf{p}_0,t) - \rho_{-\sigma,-\sigma}(\mathbf{p}_0,\mathbf{p}_0,t)], \quad (20)$$

where

$$F(\mathbf{p}_0,t) = -\frac{eE(t)p_{0y}}{[p_{0x} + p_E(t)]^2 + p_{0y}^2} \quad (21)$$

and

$$\tilde{\mathcal{E}}_{\sigma}(\mathbf{p}_0, t) = \sigma v_F \sqrt{[p_{0x} + p_E(t)]^2 + p_{0y}^2}. \quad (22)$$

Taking into account Eq. (18), it is easy to see that

$$\rho_{\sigma, \sigma'}(\mathbf{p}_0, \mathbf{p}_0, 0) = \rho_{\sigma, \sigma'}(\mathbf{p}, \mathbf{p}, 0). \quad (23)$$

To be more precise, in the set of equations (16) and (17) one should add the terms describing relaxation processes. Since we have not taken into account the relaxation processes, this consideration is correct only for the times $t < \tau_{\min}$, where τ_{\min} is the minimum of all relaxation times. Thus, full dynamics in the absence of any losses is now governed by Eqs. (19) and (20). These equations yield the conservation law for the particle number:

$$\rho_{1,1}(\mathbf{p}_0, \mathbf{p}_0, t) + \rho_{-1,-1}(\mathbf{p}_0, \mathbf{p}_0, t) = \rho_{1,1}(\mathbf{p}_0, \mathbf{p}_0, 0) + \rho_{-1,-1}(\mathbf{p}_0, \mathbf{p}_0, 0) \equiv \Xi(p_0, \mu, T). \quad (24)$$

Here we have introduced the notation $\Xi_{p_0, \mu, T}$, which, according to Eq. (14), is

$$\Xi_{p_0, \mu, T} = \frac{1}{1 + e^{\frac{v_F p_0 - \mu}{T}}} + \frac{1}{1 + e^{-\frac{v_F p_0 - \mu}{T}}}.$$

In Eqs. (19) and (20), the diagonal elements represent particle $\mathcal{N}(\mathbf{p}_0, t) \equiv \rho_{1,1}(\mathbf{p}_0, \mathbf{p}_0, t)$ and hole $\mathcal{N}_h(\mathbf{p}_0, t) = 1 - \rho_{-1,-1}(\mathbf{p}_0, \mathbf{p}_0, t)$ distribution functions, while the nondiagonal elements $\rho_{1,-1}(\mathbf{p}_0, \mathbf{p}_0, t) = \rho_{-1,1}^*(\mathbf{p}_0, \mathbf{p}_0, t)$ describe particle-hole coherent transitions. Introducing in the interaction picture the interband coherence $\mathcal{J}(\mathbf{p}_0, t)$,

$$\rho_{1,-1}(\mathbf{p}_0, \mathbf{p}_0, t) = i \mathcal{J}(\mathbf{p}_0, t) \exp \left\{ -i \frac{2}{\hbar} \int_0^t \tilde{\mathcal{E}}_1(\mathbf{p}_0, t') dt' \right\},$$

and taking into account that $\rho_{-1,-1}(\mathbf{p}_0, \mathbf{p}_0, t) = \Xi_{p_0, \mu, T} - \mathcal{N}(\mathbf{p}_0, t)$, from Eqs. (19) and (20) we obtain the following set of equations:

$$\frac{\partial \mathcal{N}(\mathbf{p}_0, t)}{\partial t} = -\frac{1}{2} F(\mathbf{p}_0, t) \left[\mathcal{J}(\mathbf{p}_0, t) \exp \left\{ -i \frac{2}{\hbar} \int_0^t \tilde{\mathcal{E}}_1(\mathbf{p}_0, t') dt' \right\} + \text{c.c.} \right], \quad (25)$$

$$\frac{\partial \mathcal{J}(\mathbf{p}_0, t)}{\partial t} = \frac{1}{2} F(\mathbf{p}_0, t) \exp \left\{ i \frac{2}{\hbar} \int_0^t \tilde{\mathcal{E}}_1(\mathbf{p}_0, t') dt' \right\} [2\mathcal{N}(\mathbf{p}_0, t) - \Xi_{p_0, \mu, T}]. \quad (26)$$

This set of equations should be solved with the initial conditions

$$\mathcal{J}(\mathbf{p}_0, 0) = 0, \quad \mathcal{N}(\mathbf{p}_0, 0) = \frac{1}{1 + e^{\frac{v_F p_0 - \mu}{T}}}. \quad (27)$$

As was mentioned in the Introduction, at the multiphoton resonant excitation, the particle-hole transitions will cause intense coherent radiation on the harmonics of the applied wave field. For the coherent part of the radiation spectrum, one needs the mean value of the current density operator along the polarization direction \hat{x} of the pump wave: $\hat{j}_x = -e v_F \langle \hat{\Psi} | \sigma_x | \hat{\Psi} \rangle$. With the help of Eqs. (4) and (12), the expectation value of the total current can be written as

$$j_x(t) = -\frac{e v_F g_s g_v S}{(2\pi\hbar)^2} \int d\mathbf{p} \{ [\rho_{11}(\mathbf{p}, \mathbf{p}, t) - \rho_{-1,-1}(\mathbf{p}, \mathbf{p}, t)] \cos \Theta(\mathbf{p}) + i \sin \Theta(\mathbf{p}) [\rho_{1,-1}(\mathbf{p}, \mathbf{p}, t) - \rho_{-1,1}^*(\mathbf{p}, \mathbf{p}, t)] \}, \quad (28)$$

where $g_s = 2$ and $g_v = 2$ are the spin and valley degeneracy factors, respectively. Taking into account Eq. (18), one can express the total current via interband coherence and particle/hole distribution functions:

$$j_x(t) = \frac{e v_F g_s g_v S}{(2\pi\hbar)^2} \int \frac{d\mathbf{p}_0}{\sqrt{[p_{0x} + p_E(t)]^2 + p_{0y}^2}} \times \left[p_{0y} \left(\mathcal{J}(\mathbf{p}_0, t) \exp \left\{ -i \frac{2}{\hbar} \int_0^t \tilde{\mathcal{E}}_1(\mathbf{p}_0, t') dt' \right\} + \text{c.c.} \right) - [p_{0x} + p_E(t)] [\mathcal{N}(\mathbf{p}_0, t) + \mathcal{N}_h(\mathbf{p}_0, t)] \right]. \quad (29)$$

From Eq. (29), it is easy to see that

$$\frac{j_x}{j_0} = f \left(\omega t; \chi_0, \frac{\mu}{\hbar\omega}, \frac{T}{\hbar\omega} \right), \quad j_0 = \frac{e\omega^2 S}{\pi^2 v_F}, \quad (30)$$

where f is the dimensionless periodic (for monochromatic wave) function, which depends parametrically on the interaction parameter $\chi_0 = eE_0 v_F / (\hbar\omega^2)$ and scaled macroscopic parameters of the system. Thus, having solutions of

Eqs. (25) and (26) and making an integration in Eq. (29), one can calculate the harmonic radiation spectrum with the help of the Fourier transform of the total current $j_x(t)$.

III. MULTIPHOTON RESONANT EXCITATION

Equations (25) and (26) represent a linear set of equations with periodic coefficients, which are analogous to Bloch equations,²⁴ describing Rabi oscillation of states' populations of two-level atomic system under resonant excitation. Note that there are significant differences between the usual Bloch equations and Eqs. (25) and (26). Thus, as is seen from Eqs. (25) and (26), the coupling term

$$\Lambda(\mathbf{p}_0, t) = F(\mathbf{p}_0, t) \exp \left\{ i \frac{2}{\hbar} \int_0^t \tilde{\mathcal{E}}_1(\mathbf{p}_0, t') dt' \right\} \quad (31)$$

is a quasiperiodic function, that is,

$$\Lambda \left(\mathbf{p}_0, t + \frac{2\pi}{\omega} \right) = \exp \left\{ i \frac{2\mathcal{E}_{E_0}(\mathbf{p}_0)}{\hbar} \frac{2\pi}{\omega} \right\} \Lambda(\mathbf{p}_0, t). \quad (32)$$

Here

$$\begin{aligned} \mathcal{E}_{E_0}(\mathbf{p}_0) &= \frac{\omega}{2\pi} \int_0^{2\pi/\omega} \tilde{\mathcal{E}}_1(\mathbf{p}_0, t) dt \\ &= v_F \frac{\omega}{2\pi} \int_0^{2\pi/\omega} \sqrt{\left(p_{0x} - \frac{eE_0}{\omega} \sin \omega t \right)^2 + p_{0y}^2} dt \end{aligned} \quad (33)$$

is the mean value of classical energy in the field (1). From the Floquet theorem and Eq. (32), it follows that instead of stationary levels $v_F p_0$ and $-v_F p_0$, due to the free-free intraband transitions we have quasistationary states with quasienergies $\pm \mathcal{E}_{E_0}(\mathbf{p}_0)$, which have a nonlinear dependence on the amplitude of the wave field. The latter, in the physical sense, is the dynamic Stark shift due to the free-free intraband transitions. Note that the definition of quasienergies is not unique, since Eq. (32) is also satisfied for $\mathcal{E}_{E_0}(\mathbf{p}_0) + s\hbar\omega$, with integer number s . Hence, we have two Floquet ladders: $\tilde{\mathcal{E}}_{\pm}(s) = \pm \mathcal{E}_{E_0}(\mathbf{p}_0) + s\hbar\omega$; $s = 0, \pm 1, \pm 2, \dots$. These ladders are coupled by the term $F(\mathbf{p}_0, t + 2\pi/\omega) = F(\mathbf{p}_0, t)$, which in turn contains all harmonics of the driving field. In the usual Bloch equations, coupling contains only fundamental oscillations, which provide only direct one-photon resonant excitation. This situation is analogous to resonant excitation of systems with permanent dipole moments, where, as has been shown in Ref. 29, it is possible to decouple slow and rapid oscillations and to disclose the resonant dynamics of the wave-particle interaction.

Because of the space homogeneity of the field (1), the generalized momentum of a particle is conserved, so that the real transitions in the field occur from a $-\mathcal{E}_{E_0}(\mathbf{p}_0)$ negative energy level to a positive $+\mathcal{E}_{E_0}(\mathbf{p}_0)$ energy level, and, consequently, the multiphoton probabilities of particle-hole pair production will have maximal values for the resonant transitions,

$$2\mathcal{E}_{E_0} \simeq n\hbar\omega, \quad n = 1, 2, 3, \dots \quad (34)$$

Note that the resonant condition (34) is equivalent to the crossing of Floquet ladders: $\tilde{\mathcal{E}}_-(s+n) \simeq \tilde{\mathcal{E}}_+(s)$. Figure 1 schematically illustrates the multiphoton interband transition between the two states in the filled lower cone and the empty part of the upper cone. Here, in contrast to resonant transitions in atomic systems with discrete energy levels, when $\hbar\omega > \mu$, the band structure of graphene is always resonant to pump

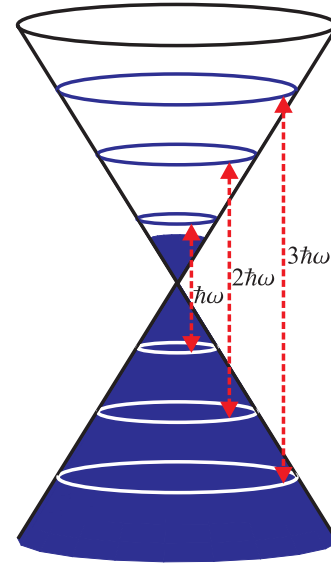


FIG. 1. (Color online) Graphene conical dispersion with interband multiphoton transitions induced by external electric field.

radiation, and with the fixed photon energies we have fixed resonant energy bands $|\mathcal{E}_{E_0} - n\hbar\omega/2| \lesssim \hbar\Omega_n$. The widths of these bands are determined by the Rabi frequency Ω_n of flopping between the two states in the lower and upper cones.

To decouple slow and rapid oscillations in Eqs. (25) and (26) at the resonant condition (34), we follow the ansatz developed in Ref. 29. Taking into account the periodicity of the function $\exp\{-2i\mathcal{E}_{E_0}(\mathbf{p}_0)t/\hbar\}\Lambda(\mathbf{p}_0, t)$ and using the Fourier series expansion of the latter,

$$\begin{aligned} e^{-\frac{2i}{\hbar}\mathcal{E}_{E_0}(\mathbf{p}_0)t} \Lambda(\mathbf{p}_0, t) &= F(\mathbf{p}_0, t) e^{i\frac{2}{\hbar} \int_0^t [\tilde{\mathcal{E}}_1(\mathbf{p}_0, t') - \mathcal{E}_{E_0}(\mathbf{p}_0)] dt'} \\ &= \sum_s G_s(\mathbf{p}_0, E_0) e^{-is\omega t}, \end{aligned} \quad (35)$$

one can represent Eqs. (25) and (26) in the form

$$\begin{aligned} \frac{\partial \mathcal{N}(\mathbf{p}_0, t)}{\partial t} &= -\frac{1}{2} \mathcal{J}(\mathbf{p}_0, t) \sum_s G_s^*(\mathbf{p}_0, E_0) \\ &\times e^{-i(\frac{2}{\hbar}\mathcal{E}_{E_0}(\mathbf{p}_0) - s\omega)t} + \text{c.c.}, \end{aligned} \quad (36)$$

$$\begin{aligned} \frac{\partial \mathcal{J}(\mathbf{p}_0, t)}{\partial t} &= \frac{1}{2} \sum_s G_s(\mathbf{p}_0, E_0) e^{i(\frac{2}{\hbar}\mathcal{E}_{E_0}(\mathbf{p}_0) - s\omega)t} \\ &\times [2\mathcal{N}(\mathbf{p}_0, t) - \Xi_{p_0, \mu, T}]. \end{aligned} \quad (37)$$

Here, the s photon coupling coefficient is

$$\begin{aligned} G_s(\mathbf{p}_0, E_0) &= \frac{\omega}{2\pi} \int_0^{2\pi/\omega} F(\mathbf{p}_0, t) \\ &\times \exp \left\{ -\sum_{m \neq 0} \frac{2\mathcal{E}_m(\mathbf{p}_0)}{m\hbar\omega} e^{-im\omega t} \right\} e^{is\omega t} dt, \end{aligned} \quad (38)$$

where

$$\mathcal{E}_m(\mathbf{p}_0) = \frac{\omega}{2\pi} \int_0^{2\pi/\omega} \tilde{\mathcal{E}}_1(\mathbf{p}_0, t) e^{im\omega t} dt. \quad (39)$$

Close to resonance (34), the main coupling term in Eqs. (36) and (37) becomes a slowly varying term with $s = n$. The

remaining nonresonant and rapidly oscillating terms are responsible only for dynamic Stark shifts.²⁹ Thus, for time-average functions $\overline{\mathcal{N}}(\mathbf{p}_0, t)$ and $\overline{\mathcal{J}}(\mathbf{p}_0, t)$, one can obtain the following set of equations:

$$\begin{aligned} \frac{\partial \overline{\mathcal{N}}(\mathbf{p}_0, t)}{\partial t} &= -\frac{1}{2} \overline{\mathcal{J}}(\mathbf{p}_0, t) G_n^*(\mathbf{p}_0, E_0) e^{-i\delta_n t} + \text{c.c.}, \\ &\times \frac{\partial \overline{\mathcal{J}}(\mathbf{p}_0, t)}{\partial t} + i\delta_{\text{St}} \overline{\mathcal{J}}(\mathbf{p}_0, t) \end{aligned} \quad (40)$$

$$= \frac{1}{2} G_n(\mathbf{p}_0, E_0) e^{i\delta_n t} [2\overline{\mathcal{N}}(\mathbf{p}_0, t) - \Xi_{p_0, \mu, T}]. \quad (41)$$

Here we have introduced resonance detuning

$$\delta_n = \frac{2\mathcal{E}_E(\mathbf{p}_0) - n\hbar\omega}{\hbar} \quad (42)$$

and the dynamic Stark shift

$$\delta_{\text{St}} = \frac{1}{2\omega} \sum_{s \neq n} \frac{|G_s(\mathbf{p}_0, E_0)|^2}{(n-s)}. \quad (43)$$

The latter is the result of a virtual nonresonant transition within Floquet states. Thus, we have a set of linear ordinary differential equations, the solution of which at the initial condition (27) is

$$\begin{aligned} \overline{\mathcal{J}}(\mathbf{p}_0, t) &= e^{i\delta_n t} \frac{G_n(\mathbf{p}_0, E_0)}{2\Omega_n} \Delta_{p_0, \mu, T} \\ &\times \left(\sin \Omega_n t - i \frac{\delta_n + \delta_{\text{St}}}{\Omega_n} (1 - \cos \Omega_n t) \right), \end{aligned} \quad (44)$$

$$\begin{aligned} \overline{\mathcal{N}}(\mathbf{p}_0, t) &= \frac{\Xi_{p_0, \mu, T}}{2} + \frac{|G_n(\mathbf{p}_0, E_0)|^2}{2\Omega_n^2} \Delta_{p_0, \mu, T} \\ &\times \left[\frac{(\delta_n + \delta_{\text{St}})^2}{|G_n(\mathbf{p}_0, E_0)|^2} + \cos \Omega_n t \right], \end{aligned} \quad (45)$$

where

$$\Delta_{p_0, \mu, T} = \frac{1}{1 + e^{\frac{\nu_F p_0 - \mu}{T}}} - \frac{1}{1 + e^{\frac{-\nu_F p_0 - \mu}{T}}} \quad (46)$$

is the initial population inversion, and

$$\Omega_n = \sqrt{|G_n(\mathbf{p}_0, E_0)|^2 + (\delta_n + \delta_{\text{St}})^2} \quad (47)$$

is the generalized Rabi frequency. The solution (45) expresses Rabi flopping among the particle-hole states at the multiphoton resonance. The solutions (44) and (45) have been derived using the assumption that $\overline{\mathcal{N}}(\mathbf{p}_0, t)$ and $\overline{\mathcal{J}}(\mathbf{p}_0, t)$ are slowly varying functions on the scale of the wave period, which establish the restrictions

$$(|G_n(\mathbf{p}_0, E_0)|, |\delta_n|, |\delta_{\text{St}}|) \ll \omega \quad (48)$$

on the characteristic parameters of the system considered.

For the exact resonant energies ($\delta_n + \delta_{\text{St}} = 0$), we have $\Omega_n = |G_n(\mathbf{p}_0, E_0)|$ and the solutions become

$$\overline{\mathcal{J}}(\mathbf{p}_0, t) = \frac{\Delta_{p_0, \mu, T}}{2} e^{i \arg[G_n(\mathbf{p}_0, E_0)]} \sin \Omega_n t, \quad (49)$$

$$\overline{\mathcal{N}}(\mathbf{p}_0, t) = \frac{\Delta_{p_0, \mu, T}}{2} \cos \Omega_n t + \frac{\Xi_{p_0, \mu, T}}{2}. \quad (50)$$

For the weak pump fields $\chi_0 \ll 1$ and one-photon interband excitation, one can omit nonlinear over E_0 terms in Eq. (38),

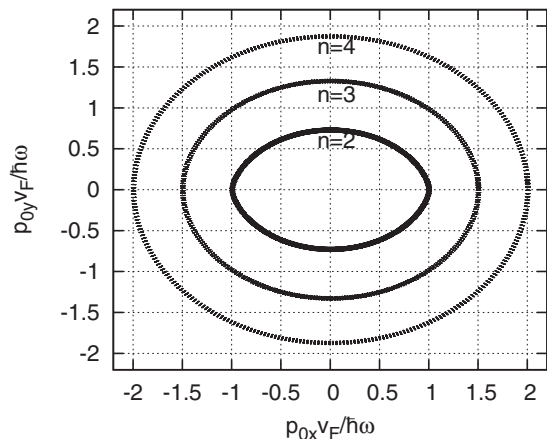


FIG. 2. Isolines of quasienergy corresponding to resonant condition $2\mathcal{E}_{E_0}(\mathbf{p}_0)/\hbar\omega \approx n$ (34) with detuning $|\delta_n|/\omega = 0.02$ for $n = 2, 3, 4$. The electric-field dimensionless parameter is taken to be $\chi_0 = 1.0$. The momentum components are normalized to $\hbar\omega/v_F$.

and for the Rabi frequency we have

$$\Omega_1 = \frac{eE_0 |\sin \Theta(\mathbf{p}_0)|}{2p_0}.$$

Taking into account the resonant condition $2p_0 v_F \simeq \hbar\omega$, the latter can be expressed through the interaction parameter χ_0 :

$$\Omega_1 = \omega |\sin \Theta(\mathbf{p}_0)| \chi_0.$$

With increasing pump wave intensity, the Rabi oscillations appear to correspond with multiphoton transitions. For strong fields, the intensity effect of the pump wave on the quasienergy spectrum (Stark shift due to free-free intraband transitions) and the dynamic Stark shift due to virtual nonresonant transitions become essential. For $\chi \sim 1$, the probabilities of multiphoton transitions are essential up to photon numbers $n \sim 5$. For these photon numbers, the Stark shift (44) is not essential, while the modification in the quasienergy spectrum is considerable. Isolines of the quasienergy spectrum, defined by Eq. (33), are no longer circles but ellipse-like because of anisotropic deformation in the linearly polarized pump wave. In Fig. 2, isolines of quasienergy corresponding to the resonant condition $2\mathcal{E}_{E_0}(\mathbf{p}_0)/\hbar\omega \approx n$ (34) with detuning $|\delta_n|/\omega = 0.02$ for $n = 2, 3, 4$ are shown in the multiphoton interaction regime: $\chi_0 = 1$. As is seen, modification of the unperturbed energy spectrum in the direction perpendicular to the electric field vector is considerable (for example, at $n = 3$ we have 13% deviation). Thus, in the multiphoton interaction regime, one should expect photoexcitation of the particle distribution function just along the modified isolines, in accordance with Eq. (50).

IV. NUMERICAL TREATMENT

We have also integrated Eqs. (25) and (26) with the fourth-order adaptive Runge-Kutta method and performed numerical simulations. Since we are mainly interested in interband multiphoton transitions, the chemical potential and temperature are fixed and are taken to be $\mu/\hbar\omega = 0.1$ and $T/\hbar\omega = 5 \times 10^{-3}$ for all calculations.

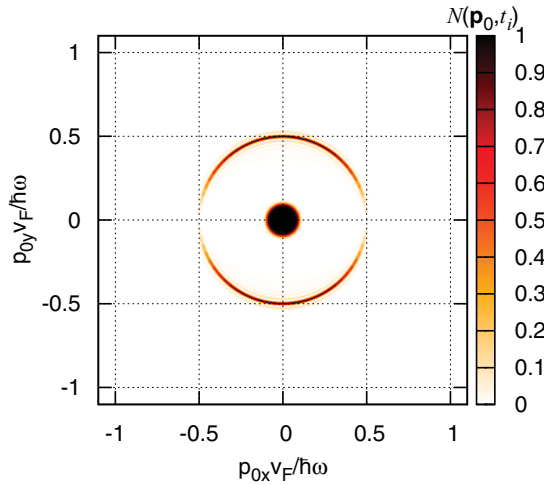


FIG. 3. (Color online) Creation of particle-hole pair in graphene at the one-photon resonant excitation. Particle distribution function $\mathcal{N}(\mathbf{p}_0, t)$ (in arbitrary units) at instant $t_i = 25T$ as a function of scaled dimensionless momentum components $\{p_{0x}v_F/\hbar\omega, p_{0y}v_F/\hbar\omega\}$. The electric-field dimensionless parameter is $\chi_0 = 0.02$.

In Figs. 3–5, the photoexcitations of the Fermi-Dirac sea are presented: the density plot of the particle distribution function $\mathcal{N}(\mathbf{p}_0, t)$ is shown for various pump wave intensities and instants. In Fig. 3, corresponding to $\chi_0 = 0.02$, we see only the creation of a particle-hole pair in graphene at the one-photon resonant excitation. In Fig. 4, the pump wave intensity is larger, $\chi_0 = 0.5$, and, as a consequence, we see resonant rings corresponding to multiphoton excitation up to four photons. In Fig. 5, which corresponds to $\chi_0 = 1$, the ring for the five-photon resonance is also clearly seen. As a result, the ring for the one-photon excitation is smeared because the Stark shift for this energy is comparable to $\hbar\omega$ and the condition (48) for resonant Rabi oscillations at one-photon excitation is not fulfilled. As is seen from Figs. 4 and 5, the excitation of the Fermi-Dirac sea takes place along the

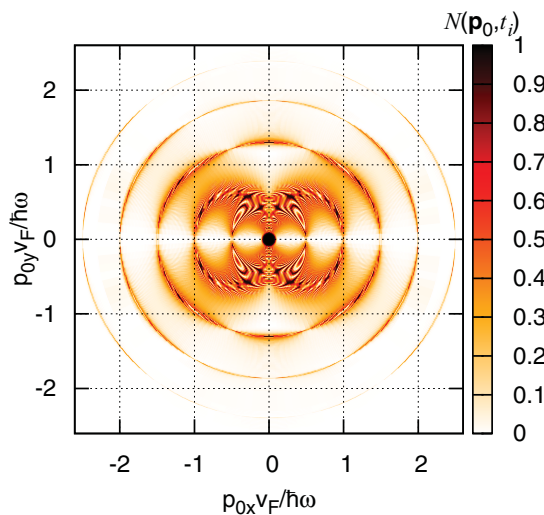


FIG. 4. (Color online) Same as Fig. 4 but for stronger wave field with $\chi_0 = 1$.

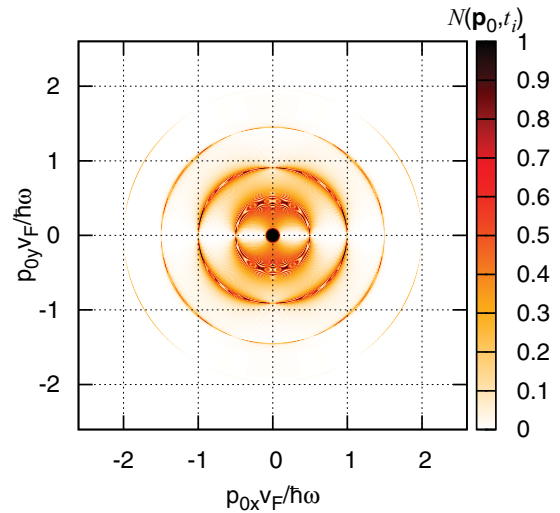


FIG. 5. (Color online) Creation of particle-hole pair in graphene at the multiphoton resonant excitation. Particle distribution function $\mathcal{N}(\mathbf{p}_0, t)$ (in arbitrary units) at instant $t_i = 100T$ as a function of dimensionless momentum components $\{p_{0x}v_F/\hbar\omega, p_{0y}v_F/\hbar\omega\}$. The electric-field dimensionless parameter is $\chi_0 = 0.5$.

ellipse-like isolines of the quasienergy spectrum defined by Eq. (33), in accordance with analytical treatment (see Fig. 2).

To show the dynamics of multiphoton excitation of the Fermi-Dirac sea in Figs. 6–8, we present Rabi oscillations of the particle distribution function $\mathcal{N}(p_0, t)$ for the fixed angles versus the scaled dimensionless momentum $p_0v_F/\hbar\omega$. Figure 6 corresponds to two-photon resonance for the angle $\Theta(\mathbf{p}_0) = 0.2$ rad and $\chi_0 = 0.5$. Rabi oscillations of $\mathcal{N}(p_0, t)$ can be clearly seen with the mean period $T_R = 22T$ ($T = 2\pi/\omega$ is the wave period). Rabi oscillations for three-photon resonance are displayed in Fig. 7 for the angle $\Theta(\mathbf{p}_0) = \pi/2$ rad and $\chi_0 = 1$. Here, the mean Rabi period is $T_R = 15T$. Four-photon resonant Rabi oscillations with the mean period $T_R = 28T$, at the angle $\Theta(\mathbf{p}_0) = 0.6$ rad, are shown in Fig. 8.

To show the dependence of Rabi oscillations on the angle $\Theta(\mathbf{p}_0)$, in Figs. 9 and 10 the colored four-dimensional (4D) density plot of Rabi oscillations of the particle resonant

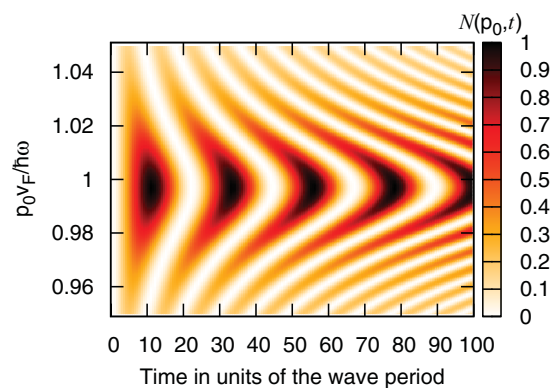


FIG. 6. (Color online) Two-photon resonance ($n = 2$). Rabi oscillations of the particle distribution function $\mathcal{N}(p_0, t)$ for the fixed angle $\Theta(\mathbf{p}_0) = 0.2$ rad vs the scaled dimensionless momentum $p_0v_F/\hbar\omega$. The electric-field dimensionless parameter is $\chi_0 = 0.5$.

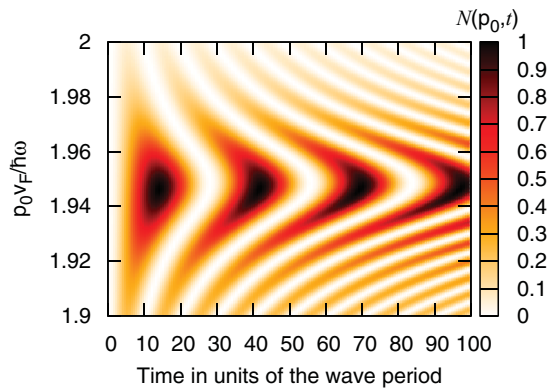


FIG. 7. (Color online) Four-photon resonance ($n = 4$). Same as Fig. 7 but for the angle $\Theta(\mathbf{p}_0) = 0.6$ rad. The electric-field dimensionless parameter is $\chi_0 = 1.0$.

distribution function $\mathcal{N}_r(\mathbf{p}_0, t)$ on isosurfaces $2\mathcal{E}_{E_0}(\mathbf{p}_0)/\hbar\omega = n$ for $n = 3, 4$ are shown at $\chi_0 = 1$. As is seen from these figures, for odd photon resonance the excited distribution function $\mathcal{N}_r(\mathbf{p}_0, t)$ is maximal at the angle $\Theta(\mathbf{p}_0) = \pi/2$ rad (perpendicular to the applied electric field vector), while for even photon resonance at $\Theta(\mathbf{p}_0) = \pi/2$ rad we have a minimum, and the main excitation takes place close to $\Theta(\mathbf{p}_0) = \pi/4$. The latter is connected to the fact that the coupling term in Eqs. (36) and (37) at $\Theta(\mathbf{p}_0) = \pi/2$ rad contains only odd harmonics of the pump wave: $G_{2s}(0, p_{0y}, E_0) = 0$.

Note that the described Rabi oscillations of the particle distribution function may be experimentally probed by pump-probe, time-resolved photoemission spectroscopy.^{39,40} Another observable process in the scope of described nonlinear dynamics is the harmonic radiation. Therefore, we proceed to a harmonic radiation spectrum which can be calculated with the help of the Fourier transform of $j_x(t)$. As is clear from Eq. (29), the spectrum contains in general both even and odd harmonics. However, depending on the initial conditions, particularly for the equilibrium initial state (27) and smooth turn-on/off of the wave field, the terms containing even harmonics cancel each other, and only the odd harmonics are generated. For turn-on/off of the wave field, the latter is described by the envelope $\sin^2(\pi t/T_p)$ (for the time period

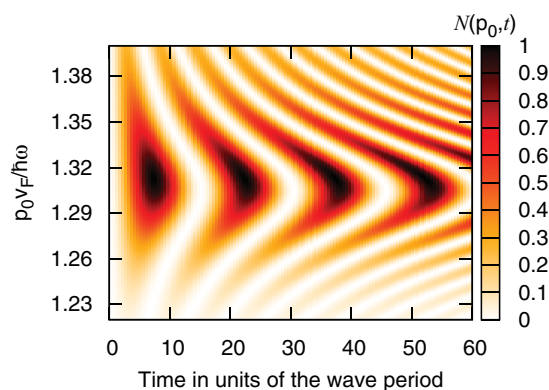


FIG. 8. (Color online) Same as Fig. 6 but for three-photon resonance ($n = 3$). The angle is taken to be $\Theta(\mathbf{p}_0) = \pi/2$ rad. The electric-field dimensionless parameter is $\chi_0 = 1.0$.

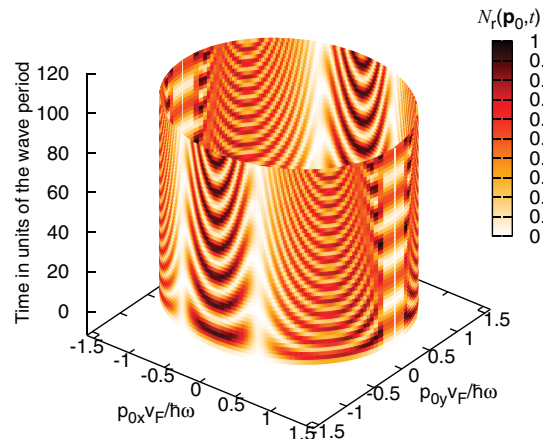


FIG. 9. (Color online) Colored 4D plot of Rabi oscillations of the particle distribution function $\mathcal{N}_r(\mathbf{p}_0, t)$ for three-photon resonance on isosurface $2\mathcal{E}_{E_0}(\mathbf{p}_0)/\hbar\omega = 3$. The electric-field dimensionless parameter is $\chi_0 = 1.0$.

$0 \leq t \leq T_p$), where T_p characterizes the pulse duration, and it is chosen to be $T_p = 32T$. The emission rate of the N th harmonic is proportional to $N^2|j_N|^2$, where j_N is the N th Fourier component of the field-induced current (29). To find out j_N , the fast Fourier transform algorithm has been used.

Figure 11 displays the harmonic emission rate via $\log_{10}(N^2|f_N|^2)$, where f_N is the N th Fourier component of the normalized current (30). To estimate the considered effect, we present the results of numerical calculations for a relatively weak wave field as well. As we see from this figure, for weak fields the full radiation is concentrated on the incident radiation frequency. For strong fields, the peaks appear in the spectrum corresponding to harmonics emission (up to seventh harmonic). Even harmonics, as well as the low-frequency radiation corresponding to Rabi oscillations,³¹ are absent because of inversion symmetry. Assuming the dipole radiation mechanism, the conversion efficiency for harmonics $\eta_n = I_n/I$ can be estimated as $\eta_n \sim 10^{-3}\chi_0^{-2}(d/\lambda)^2 N^2|f_N|^2$, where $\lambda = 2\pi c/\omega$ and $d = \min\{L_g, w\}$, with L_g and w being the characteristic sizes of graphene and the laser beam waist,

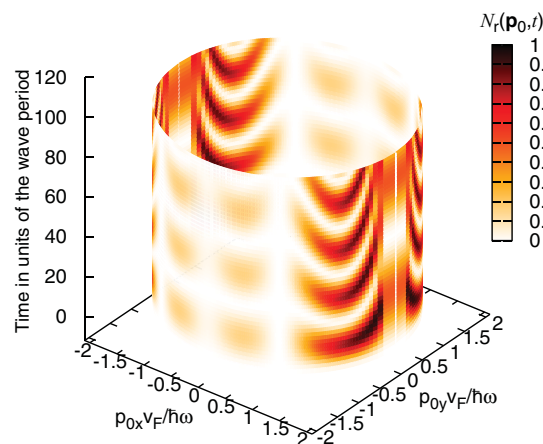


FIG. 10. (Color online) Same as Fig. 9 but for four-photon resonance: $2\mathcal{E}_{E_0}(\mathbf{p}_0)/\hbar\omega = 4$.

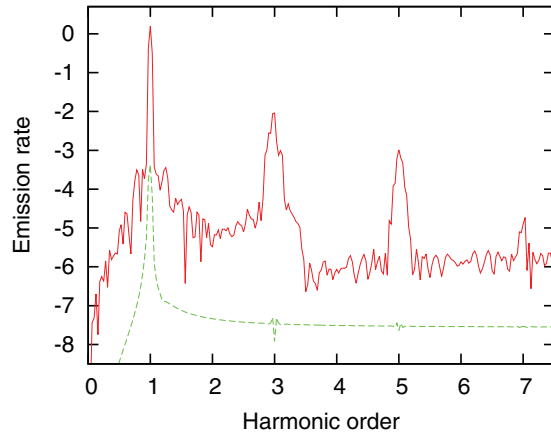


FIG. 11. (Color online) Harmonic emission rate in graphene at the resonant excitation via $\log_{10}(N^2|f_N|^2)$ (in arbitrary units) as a function of the photon energy (in units of $\hbar\omega$). The solid (red) line corresponds to the electric-field dimensionless parameter $\chi_0 = 1$; the dashed (green) line corresponds to $\chi_0 = 0.02$.

respectively. For the setup of Fig. 11, depending on the ratio d/λ , one can achieve quite large conversion efficiencies for third and fifth harmonics, which are comparable to what one expects to achieve with resonant two-level systems.^{30,32,41}

Summarizing, we see that numerical simulations are in agreement with analytical treatment in the multiphoton resonant approximation and confirm the revealed physical picture described in the preceding section. We see that with laser fields of moderate intensities, one can observe the resonant multiphoton excitation of the Fermi-Dirac sea and efficient generation of moderately high harmonics in graphene.

V. CONCLUSION

We have presented a theoretical treatment of the coherent nonlinear response of graphene under multiphoton interband excitation by laser radiation of moderate intensities. The evolutionary equation for a single-particle density matrix is formulated arising from the second quantized formalism. The time-dependent single-particle density matrix in the given field of laser radiation is calculated in the multiphoton resonant approximation. The Rabi oscillations of the Fermi-Dirac sea at multiphoton excitation depending on the time, momentum, and photons number have been considered and analyzed also on the basis of numerical simulations. The results obtained demonstrate Rabi oscillations of the Fermi-Dirac sea in the graphene corresponding to multiphoton excitation that can already be observed for such laser fields where the effect of the electric field on the wave period is comparable to photon energy $\varepsilon_\gamma = \hbar\omega$. For the midinfrared lasers $\varepsilon_\gamma \sim 0.1$ eV, the multiphoton interaction regime can be achieved at the intensities $I > 10^7$ W cm⁻² for the time scales 1.0 ps. For the near-infrared range of frequencies $\varepsilon_\gamma \sim 1$ eV, the multiphoton interaction regime can be achieved at the intensities $I > 10^{11}$ W cm⁻² for the time scales 100.0 fs. Hence, the described Rabi oscillations of the particle distribution function may be experimentally probed by pump-probe, picosecond, or femtosecond time-resolved photoemission spectroscopy.^{39,40} In addition, along with Rabi oscillations one can achieve efficient generation of harmonics with laser fields of moderate intensities.

ACKNOWLEDGMENTS

This work was supported by State Committee of Science (SCS) of the Republic of Armenia (RA), Project No. 11RB-006.

*avetissian@ysu.am

¹K. S. Novoselov, A. K. Geim, S. V. Morozov, D. Jiang, Y. Zhang, S. V. Dubonos, I. V. Grigorieva, and A. A. Firsov, *Science* **306**, 666 (2004).

²A. H. Castro Neto, F. Guinea, N. M. R. Peres, K. S. Novoselov, and A. K. Geim, *Rev. Mod. Phys.* **81**, 109 (2009).

³A. K. Geim, *Science* **324**, 1530 (2009).

⁴K. S. Novoselov, A. K. Geim, S. V. Morozov, D. Jiang, M. I. Katsnelson, I. V. Grigorieva, S. V. Dubonos, and A. A. Firsov, *Nature (London)* **438**, 197 (2005).

⁵G. W. Semenoff, *Phys. Rev. Lett.* **53**, 2449 (1984).

⁶F. D. M. Haldane, *Phys. Rev. Lett.* **61**, 2015 (1988).

⁷M. I. Katsnelson, K. S. Novoselov, and A. K. Geim, *Nat. Phys.* **2**, 620 (2006).

⁸V. V. Cheianov, V. I. Fal'ko, and B. L. Altshuler, *Science* **315**, 1252 (2007).

⁹M. I. Katsnelson and K. S. Novoselov, *Solid State Commun.* **143**, 3 (2007).

¹⁰H. K. Avetissian, *Relativistic Nonlinear Electrodynamics* (Springer, New York, 2006).

¹¹M. I. Katsnelson, *Mater. Today* **10**, 20 (2007).

¹²V. V. Cheianov and V. I. Fal'ko, *Phys. Rev. B* **74**, 041403 (2006).

¹³C. W. J. Beenakker, *Rev. Mod. Phys.* **80**, 1337 (2008).

¹⁴J. Schwinger, *Phys. Rev.* **82**, 664 (1951).

¹⁵D. Allor, T. D. Cohen, and D. A. McGady, *Phys. Rev. D* **78**, 096009 (2008).

¹⁶B. Dóra and R. Moessner, *Phys. Rev. B* **81**, 165431 (2010).

¹⁷C. Itzykson and J.-B. Zubar, *Quantum Field Theory* (Dover, New York, 2006).

¹⁸M. I. Katsnelson, *Eur. Phys. J. B* **51**, 157 (2006).

¹⁹J. Cserti and Gy. Dávid, *Phys. Rev. B* **74**, 172305 (2006).

²⁰J. Schliemann, *New J. Phys.* **10**, 043024 (2008).

²¹A. W. W. Ludwig, M. P. A. Fisher, R. Shankar, and G. Grinstein, *Phys. Rev. B* **50**, 7526 (1994).

²²K. Ziegler, *Phys. Rev. B* **75**, 233407 (2007).

²³H. K. Avetissian, A. K. Avetissian, G. F. Mkrtchian, and Kh. V. Sedrakian, *Phys. Rev. E* **66**, 016502 (2002).

²⁴L. Allen and J. H. Eberly, *Optical Resonance and Two Level Atoms* (Wiley-Interscience, New York, 1975); B. W. Shore, *Theory of Coherent Atomic Excitation* (Wiley-Interscience, New York, 1990); M. O. Scully and M. S. Zubairy, *Quantum Optics* (Cambridge University Press, Cambridge, UK, 1997).

²⁵F. Rossi and T. Kuhn, *Rev. Mod. Phys.* **74**, 895 (2002); V. M. Axt and T. Kuhn, *Rep. Prog. Phys.* **67**, 433 (2004).

²⁶E. G. Mishchenko, *Phys. Rev. Lett.* **103**, 246802 (2009).

²⁷P. N. Romanets and F. T. Vasko, *Phys. Rev. B* **81**, 241411(R) (2010).

- ²⁸B. Dóra, K. Ziegler, P. Thalmeier, and M. Nakamura, *Phys. Rev. Lett.* **102**, 036803 (2009).
- ²⁹H. K. Avetissian and G. F. Mkrtchian, *Phys. Rev. A* **66**, 033403 (2002).
- ³⁰H. K. Avetissian, B. R. Avchyan, and G. F. Mkrtchian, *Phys. Rev. A* **77**, 023409 (2008).
- ³¹H. K. Avetissian, B. R. Avchyan, and G. F. Mkrtchian, *Phys. Rev. A* **82**, 063412 (2010).
- ³²H. K. Avetissian, B. R. Avchyan, and G. F. Mkrtchian, *J. Phys. B* **45**, 025402 (2012).
- ³³S. A. Mikhailov, *Europhys. Lett.* **79**, 27002 (2007).
- ³⁴S. A. Mikhailov and K. Ziegler, *J. Phys.: Condens. Matter* **20**, 384204 (2008).
- ³⁵F. J. Lopez-Rodriguez and G. G. Naumis, *Phys. Rev. B* **78**, 201406(R) (2008).
- ³⁶K. L. Ishikawa, *Phys. Rev. B* **82**, 201402(R) (2010).
- ³⁷S. A. Mikhailov, *Phys. Rev. B* **84**, 045432 (2011).
- ³⁸M. M. Glazov, *JETP Lett.* **93**, 366 (2011).
- ³⁹L. Perfetti *et al.*, *New J. Phys.* **10**, 053019 (2008).
- ⁴⁰J. K. Freericks, H. R. Krishnamurthy, and Th. Pruschke, *Phys. Rev. Lett.* **102**, 136401 (2009).
- ⁴¹R. W. Boyd, *Nonlinear Optics* (Academic, San Diego, 1992).